ε-Contributions to the Mathematical Image Processing Field

Computer Vision Group - TUM

A.Buades, B.Coll, J.Duran and C.Sbert

May 16, 2014

Invertim en el seu futur
Unió Europea
Fons Social Europeu

Govern de les Illes Balears
Conselleria d'Educació, Cultura i Universitats
Direcció General d'Universitats,
Recerca i Transferència del Coneixement

Contents

Introduction

Treatment and Mathematical Analysis of Digital Images Group (TAMI)
Department of Mathematics and Computer Sciences
University of Balearic Islands
Cra. Valldemossa, km. 7.5, Palma (Mallorca)

Introduction

TAMI members

Prof. Bartomeu Coll

Dr. Catalina Sbert

Dr. Antoni Buades

Prof. Jean-Michel Morel

Dr. José Luis Lisani

Dra. Ana Belén Petro

Introduction

TAMI research activity

Image restoration

Image demosaicking

Color restoration

Satellite pansharpening

Texture segmentation

Texture synthesis

Video, multiview reconstruction, medical imaging...

Introduction

TAMI research activity

Image restoration

Image demosaicking

Color restoration

Satellite pansharpening

Texture segmentation

Texture synthesis

Video, multiview reconstruction, medical imaging...

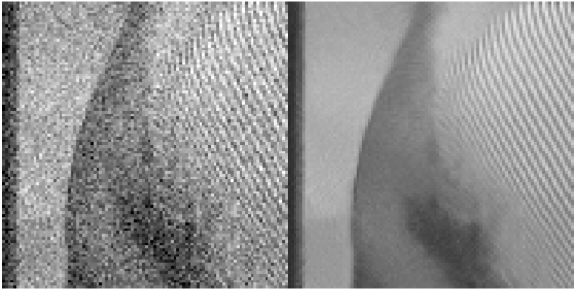

Introduction

TAMI research activity

- Image restoration
- **Image demosaicking**
- Color restoration
- Satellite pansharpening
- Texture segmentation
- Texture synthesis
- Video, multiview reconstruction, medical imaging...

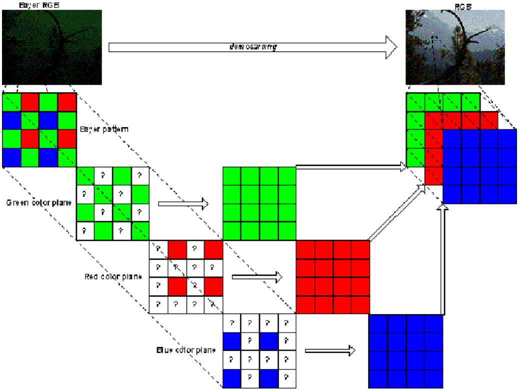

Introduction

TAMI research activity

- Image restoration
- **Image demosaicking**
- Color restoration
- Satellite pansharpening
- Texture segmentation
- Texture synthesis
- Video, multiview reconstruction, medical imaging...

Introduction

TAMI research activity

- Image restoration
- **Image demosaicking**
- Color restoration
- Satellite pansharpening
- Texture segmentation
- Texture synthesis
- Video, multiview reconstruction, medical imaging...

Introduction

TAMI research activity

- Image restoration
- Image demosaicking
- **Color restoration**
- Satellite pansharpening
- Texture segmentation
- Texture synthesis
- Video, multiview reconstruction, medical imaging...

Introduction

TAMI research activity

- Image restoration
- Image demosaicking
- **Color restoration**
- Satellite pansharpening
- Texture segmentation
- Texture synthesis
- Video, multiview reconstruction, medical imaging...

Introduction

TAMI research activity

- Image restoration
- Image demosaicking
- Color restoration
- **Satellite pansharpening**
- Texture segmentation
- Texture synthesis
- Video, multiview reconstruction, medical imaging...

Introduction

TAMI research activity

- Image restoration
- Image demosaicking
- Color restoration
- **Satellite pansharpening**
- Texture segmentation
- Texture synthesis
- Video, multiview reconstruction, medical imaging...

Introduction

TAMI research activity

- Image restoration
- Image demosaicking
- Color restoration
- **Satellite pansharpening**
- Texture segmentation
- Texture synthesis
- Video, multiview reconstruction, medical imaging...

Introduction

TAMI research activity

- Image restoration
- Image demosaicking
- Color restoration
- Satellite pansharpening
- **Texture segmentation**
- Texture synthesis
- Video, multiview reconstruction, medical imaging...

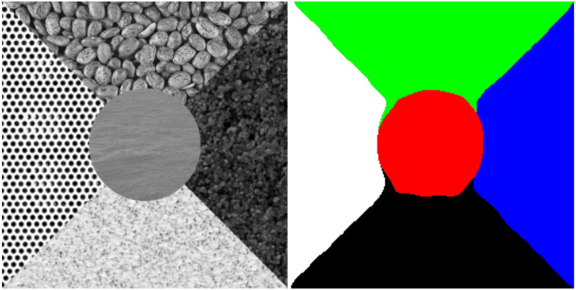

Introduction

TAMI research activity

- Image restoration
- Image demosaicking
- Color restoration
- Satellite pansharpening
- Texture segmentation
- **Texture synthesis**
- Video, multiview reconstruction, medical imaging...

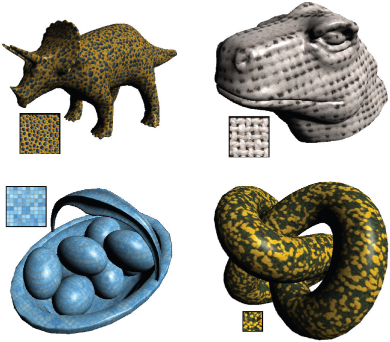

Introduction

TAMI research activity

- Image restoration
- Image demosaicking
- Color restoration
- Satellite pansharpening
- Texture segmentation
- Texture synthesis
- **Video, multiview reconstruction, medical imaging...**

Introduction

Funding projects, patents and relevant papers

Industrial activity

- We have a permanent technology transfer contract, renewed every year since 2006 with the company DxO, one of the world leaders in image processing, whose image processing chains equips currently more than 300 millions cameraphones.
- We have also been cooperating with CNES (Centre National d'Etudes Spatiales) for over one decade, where the team contributed the image restoration chain of the Earth observation satellites SPOT5 and the recently launched Pléiades.

Funding projects

- Spanish project: Restauración y análisis de imágenes digitales, Ministerio de Ciencia e Innovación (TIN2011-27539), renewed every three years since 1998.
- CNES: permanent association funded since 2007 by renewable research contracts.
- DxO: permanent contract since 2007.
- European project Eurostars: High Resolution Waferlevel reflowable EDoF Camera Module (E! 4303-WAFLE). Pathners: DxO labs, Heptagon, UIB. Coordinator: DxO Labs. Period: 2008-2010.

Patents

- A. Buades, B. Coll, J.-M. Morel, "Procédé traitement des données d'image, par réduction de bruit d'image, et caméra intégrant de moyens de mise en oeuvre du procédé". Ref PCT/FR2005/000897. Licensing agreements negotiated with: DxO (French company), LIM (Czech company), Cognitech (US company).
- F. Cao, F. Guichard, N. Azzabou, A. Buades, B. Coll, J.-M. Morel, "Procedé de traitement d'objet numerique et systeme associé", DxO company, Ref. EP2174289 A2, FR2919943-A1; WO2009022083-A2.
- G. Blanchet, A. Buades, B. Coll, J.M. Morel, B. Rougé. "Procedimiento de establecimiento de correspondencia entre una primer imagen digital y una segunda imagen digital de una misma escena para la obtención de disparidades", Spanish patent Ref. P25155ES00, Ref. PCT/ES2010/070813. Owner: UIB-CNES.
- L.I. Rudin, J.L. Lisani, J.-M. Morel, P. Yu. "Video demultiplexing based on meaningful modes extraction", EEUU Patent Ref. 7328533. Owner: Cognitec, 2010.
- L.I. Rudin, J.L. Lisani, P. Monasse, J.-M. Morel. "Object recognition based on 2D images and 3D models", EEUU Patent Ref. 7587082. Owner: Cognitec, 2010.

Relevant journal papers

- J. Duran, A. Buades, B. Coll, C. Sbert. *A nonlocal variational model for pansharpening image fusion*. SIAM J. Imaging Sci., 7(2):761-796, 2014.
- M. Lebrun, A. Buades, J.-M. Morel. *A Non-local Bayesian image denoising algorithm*. SIAM J. Imaging Sci., 6(3):1665-1688, 2013.
- A. Buades, J.-M. Morel, J.L. Lisani. *How to explore the patch space*. Inverse Problems in Imaging, 7(3):813-838, 2013.
- J.V. Manjón, P. Coupé, A. Buades, L. Collins, M. Robles. *DTI denoising using overcomplete Local PCA decomposition*. Plos One, 2013.
- J.-M. Morel, A.B. Petro, C. Sbert. *Fourier implementation of Poisson image editing*. Pattern Recognition Letters, 33: 342-348, 2012.
- J.V. Manjón, P. Coupé, A. Buades, L. Collins, M. Robles. *New methods for MRI Denoising based on Sparseness and Self-Similarity*. Medical Image Analysis, 16(1):18?27, 2012.
- L. Zhang, X. Wu, A. Buades, X. Li. *Color demosaicking by local directional interpolation and non-local enhancement with adaptive sparse representation*. J. Electronic Imaging, 20(2), 2011.
- A. Buades, J.L. Lisani, J.-M. Morel. *The dimensionality of color space in natural images*. Journal of Optical Society of America, 28(2): 203-209, 2011.
- G. Blanchet, A. Buades, B. Coll, J.-M. Morel, B. Rougé. *Fattening free correlation*. J. Math. Imaging and Vision, 41(1):109-121, 2011.
- J.-M. Morel, A.B. Petro, C. Sbert. *A PDE formalization of retinex theory*. IEEE Trans. Image Process., 19(11):2825-2837, 2010.
- A. Buades, B. Coll, J.-M. Morel, C. Sbert. *Self similarity driven demosaicking*. IEEE Trans. Image Process., 18(6):1192-1202, 2009.
- J. Delon, A. Desolneux, J.L. Lisani, A.B. Petro. *A non-parametric approach for histogram segmentation*. IEEE Trans. Image Process., 16(1): 253-261, 2007.
- A. Buades, B. Coll, J.-M. Morel. *The staircasing effect in neighborhood filters and its solution*. IEEE Trans. Image Process., 15(6):1499-1505, 2006.
- A. Buades, B. Coll, J.-M. Morel. *A review of image denoising methods, with a new one*. SIAM Multiscale Model. and Simulation, 4(2):490-530, 2005.

Introduction

In memoriam

In memory of Professor

Vicent Caselles Costa
August 10, 1960 - August 14, 2013
Gata, Alacant, Spain

- Prof. at the University of Balearic Islands (1991-1999) where he co-founded the TAMI group together with Prof. Jean-Michel Morel and Bartomeu Coll.
- **Research interests**: image segmentation, restoration, interpolation and inpainting, color image processing, optical flow computation, logo detection and shape recognition, the development of image processing tools for the media industry including the development of efficient methods for depth computation, 3D reconstruction and free-viewpoint video visualization of a 3D scene using a calibrated multi-camera set-up.
- **Life's work:** he is the author of three books and more than 120 papers published in peer-reviewed journals with more than 15.000 mentions (he is the most mentioned spanish mathematician).
- **Prizes:** third national Prize for the degree in Mathematics (1983), PhD prize of University of València (1985), Distinció de la Generalitat de Catalunya per a la recerca (2002), Ferran Sunyer i Balaguer Prize, SIAM Outstanding Paper Prize 2008, ICREA Acadèmia Prize for excellence in research of the Generalitat de Catalunya (2006), "Test of Time"Award 2011 at the International Conference on Computer Vision, and SIAM Activity Group on Imaging Science Prize (2012).
- He received the **European Research Council Advanced Grant** for "Inpainting Tools for Video Post-production. Variational theory and fast algorithms".

Vicent Caselles' legacy

- **Geodesic snakes:** a novel mathematical theory to visualize tumors from medical imaging and, thus, allowing doctors to observe and measure how they grow.
- **Image inpainting:** a novel mathematical theory to reconstruct lost or deteriorated parts of images and videos.

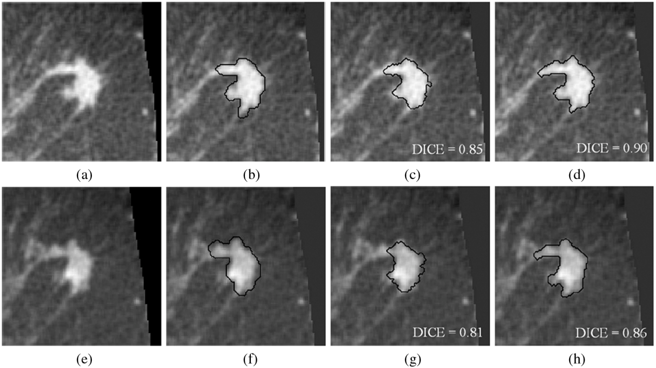

Vicent Caselles' legacy

- **Geodesic snakes:** a novel mathematical theory to visualize tumors from medical imaging and, thus, allowing doctors to observe and measure how they grow.
- **Image inpainting:** a novel mathematical theory to reconstruct lost or deteriorated parts of images and videos.

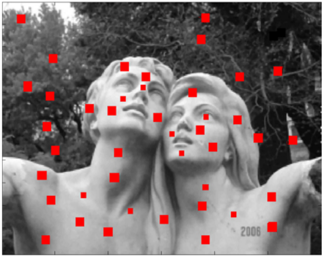

Video Inpainting

Contents

Half-linear regularization for nonconvex image restoration

The general minimization problem

Inverse problem $\rightarrow$ recover u from $f = Au + \eta$ $\rightarrow$ ill-posed problem.

Regularization $\rightarrow$ find the minimizer in $X = \mathbb{R}^{N \times N}$ of the discrete functional

$$J(u) = \underbrace{\sum_{1 \leq i,j \leq N} \phi\left(|(\nabla u)_{i,j}|\right)}_{\text{regularization term}} + \underbrace{\frac{\lambda}{2} \|Au - f\|_X^2}_{\text{data-fidelity term}}$$

- A $\rightarrow$ linear operator modeling the degradation of u.
- ϕ $\rightarrow$ nonsmooth nonconvex potential function.
- λ $\rightarrow$ positive trade-off parameter.

Theorem (Existence of minimizer)

Let $\phi : [0, +\infty) \rightarrow [0, +\infty)$ be a continuous and increasing function s.t. $\phi(0) = 0$. If ker$(A) \cap$ ker$(\nabla) = \{0\}$, then there exists $\widehat{u} \in X$ s.t. $J(\widehat{u}) = \min_{u \in X} J(u)$.

Half-linear regularization for nonconvex image restoration

Assumptions on the potential function

Euler-Lagrange equations for a formal minimizer u of J:

$$-\text{div}\left(\phi'\left(|\nabla u|\right)\frac{\nabla u}{|\nabla u|}\right) + \lambda A^*\left(Au - f\right) = 0,$$

$$A^*Au - \frac{1}{\lambda}\left(\frac{\phi'(|\nabla u|)}{|\nabla u|}u_{TT} + \phi''(|\nabla u|)u_{NN}\right) = A^*f.$$

Assumptions on ϕ

(A1) $\phi : [0,+\infty) \to [0,+\infty)$ strictly increases on $(0,+\infty)$ with $\phi(0) = 0$.

(A2) ϕ is twice continuously differentiable on $(0,+\infty)$.

(A3) ϕ' strictly decreases on $(0,+\infty)$.

(A4) $\lim_{t\to\infty} \phi'(t) = 0$.

(A5) $\lim_{t\downarrow 0^+} \phi'(t) = M$, with $0 < M < +\infty$.

Half-linear regularization for nonconvex image restoration

The basic dual theorem

Key $\rightarrow$ introduce a dual variable, with closed expression, which detects edges.

Theorem (Half-linear regularization)

Let ϕ satisfy requirements (A1)-(A5) and let M be the real value given in (A5).

i) *There exists a strictly decreasing and strictly convex function ψ such that*

$$\phi(t) = \min_{\omega \in (0,M)} \left(\omega t + \psi(\omega)\right).$$

ii) *For each $t \geq 0$, the above minimum is unique and given by $\widehat{\omega} = \phi'(t)$.*

Under conditions (A1)-(A5), the primal functional can be written as

$$J(u) = \min_{\omega \in (0,M]^{N^2}} J^*(u,\omega) = J^*\left(u, \phi'(\nabla u)\right),$$

where the dual energy is explicitly given by

$$J^*(u,\omega) = \sum_{1 \leq i,j \leq N} \left(\omega_{i,j} |(\nabla u)_{i,j}| + \psi(\omega_{i,j})\right) + \frac{\lambda}{2} \|Au - f\|_X^2.$$

$\phi(t)$	$\widehat{\omega}$	M	$\psi(\omega)$
$\phi_1(t) = \frac{t}{\sqrt{1+t^2}}$	$\frac{1}{(1+t^2)^{\frac{3}{2}}}$	1	$\left(1-\omega^{\frac{2}{3}}\right)^{\frac{3}{2}}$
$\phi_2(t) = \frac{t}{1+t}$	$\frac{1}{(1+t)^2}$	1	$\left(1-\sqrt{\omega}\right)^2$
$\phi_3(t) = \ln(1+t)$	$\frac{1}{1+t}$	1	$\omega - \ln\omega - 1$
$\phi_4(t) = (1+t)^\gamma - 1, 0<\gamma<1$	$\frac{\gamma}{(1+t)^{1-\gamma}}$	γ	$\omega - 1 + (1-\gamma)\left(\frac{\omega}{\gamma}\right)^{\frac{\gamma}{\gamma-1}}$

Table : Examples of potential functions satisfying (A1)-(A5).

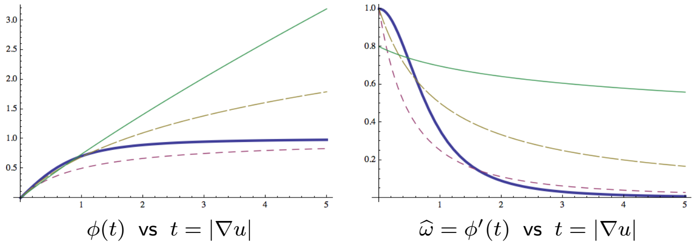

Figure : Plots of ϕ_1 (solid line), ϕ_2 (large dashed line), ϕ_3 (short dashed line) and ϕ_4 (thick line).

Half-linear regularization for nonconvex image restoration

Properties of the minimizers

- Nonconvexity gives better results than convexity for edge-preservation.
- **Claim** $\rightarrow$ fully segmented solutions of arbitrary linear inverse problems can be found by minimizing an objective functional where the regularization term is nonsmooth and nonconvex.
- **Assumption:** (A6) $\frac{\phi''(t)}{t^2}$ strictly increases on $(0, +\infty)$ and $\lim_{t \downarrow 0^+} \frac{\phi''(t)}{t^2} = -\infty$.

Theorem (Properties of minimizers)

If $\ker(A) \cap \ker(\nabla) = \{0\}$ *and (A1)-(A6) hold, then any minimizer* $\widehat{u} \in X$ *of the primal energy* J *satisfies*

$$\textit{either} \quad |(\nabla \widehat{u})_{i,j}| = 0 \quad \textit{or} \quad |(\nabla \widehat{u})_{i,j}| \geq \theta, \quad \forall\, 1 \leq i, j \leq N,$$

where $0 < \theta < +\infty$ *is the unique real value, independent of* $\widehat{u}$*, that solves the implicit equation* $\phi''(\theta) = -\lambda\mu\theta^2 \|f\|_X^2$*, with* μ *being a constant such that* $\mu \geq 1$*.*

Half-linear regularization for nonconvex image restoration

The proposed dual algorithm

- **Proposed dual algorithm**:

$$\omega^{n+1} = \arg\min_{\omega} J^*\left(u^n, \omega\right) = \phi'\left(|\nabla u^n|\right)$$
$$u^{n+1} = \arg\min_{u} J^*\left(u, \omega^{n+1}\right) \rightarrow \text{solve WTV-equation}$$

- **Convergence analysis:**
  - If $\mathcal{M}(u) = \arg\min_v J^*\left(v, \phi'(|\nabla u|)\right)$, then $u^{n+1} \in \mathcal{M}(u^n)$.
  - If $\mathcal{S} = \{u \in X : u \in \mathcal{M}(u)\}$, then $u \in \mathcal{S} \Leftrightarrow u$ is a stationary point of J.

Theorem (Convergence of the algorithm)

i) $\{J(u^n) = J^*(u^n, \omega^{n+1})\}$ *decreases and converges to* $J(\widehat{u})$, *where* $\widehat{u} \in \mathcal{S}$.

ii) $\{u^n\}$ *has convergent subsequences and their limits are stationary points of* J.

iii) *Either* $\{u^n\}$ *converges to a stationary point of* J *or its limit points form a continuum in* $\mathcal{S}$.

iv) *If all the stationary points of* J *are isolated, then* $\{u^n\}$ *converges to a stationary point of* J.

v) *There exists a sequence* $\{\widehat{u}^n\} \subset \mathcal{S}$ *such that* $\lim_{n\to\infty} \|u^n - \widehat{u}^n\|_X = 0$.

vi) *Let* $\widehat{u}$ *be any isolated stationary point of* J. *If* $\widehat{u}$ *is a strong local minimizer of* J, *then there exists an open neighbourhood* B *of* $\widehat{u}$ *such that* $\{u^n\}$ *converges to* $\widehat{u}$ *for any* $u^0 \in B$.

Half-linear regularization for nonconvex image restoration

Experimental results

Noise-free image

$\hat{\omega}$ related to ϕ_2

Noisy image

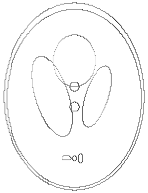

$\hat{\omega}$ related to ϕ_1

Figure : The role of the dual variable ω as edge detector

Ground truth

Blurred image

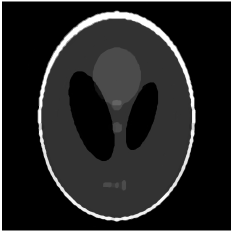

ϕ_1

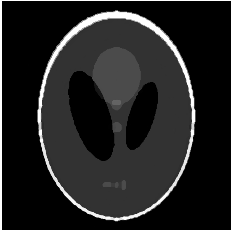

ϕ_2

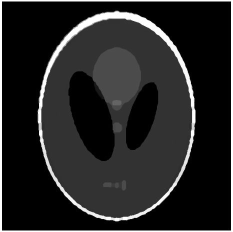

ϕ_3

$\phi_4(\gamma = 0.5)$

Figure : Deconvolution of a piecewise constant image convolved with Gaussian kernel of s.d. $\sigma = 5$

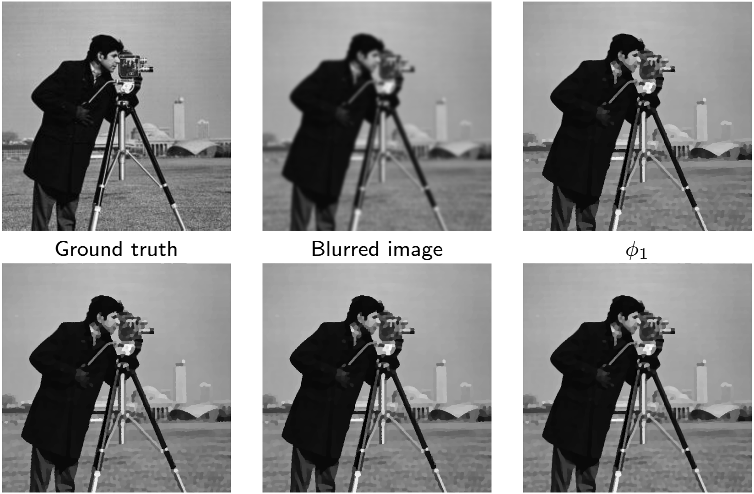

Ground truth — Blurred image — ϕ_1

ϕ_2 — ϕ_3 — $\phi_4(\gamma = 0.5)$

Figure : Deconvolution of a non-constant image convolved with Gaussian kernel of s.d. $\sigma = 3$.

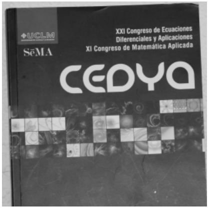

Book

Building

Cameraman

Chairs

Phantom

Testcard

Figure : Set of grayscale images used for state-of-the-art TV-based image denoising algorithms

Image	Noisy image		Chambolle		Split Bregman		Half-quadratic		Half-linear	
	RMSE	PSNR	RMSE	PSNR	RMSE	PSNR	RMSE	PSNR	RMSE	PSNR
1	17.38	24.65	7.21	31.50	8.09	30.44	7.76	31.06	**6.99**	**31.88**
2	17.03	24.82	10.50	28.38	11.23	27.79	10.34	28.73	**9.57**	**29.28**
3	16.81	24.91	9.00	29.64	10.04	28.68	8.92	29.91	**8.26**	**30.46**
4	16.47	25.03	8.80	29.98	9.95	28.93	8.62	30.27	**7.88**	**30.96**
5	14.24	26.41	7.20	32.33	9.22	30.03	5.77	34.21	**5.29**	**35.31**
6	16.89	24.85	9.80	29.26	10.85	28.30	9.31	29.68	**8.27**	**30.62**
Avg.	16.47	25.11	8.75	30.18	9.90	29.03	8.45	30.64	**7.71**	**31.42**

For each image, the averages of both the RMSE and the PSNR over all s.d. are displayed.

σ	Noisy image		Chambolle		Split Bregman		Half-quadratic		Half-linear	
	RMSE	PSNR	RMSE	PSNR	RMSE	PSNR	RMSE	PSNR	RMSE	PSNR
5	4.85	34.45	3.59	37.27	4.25	35.66	3.36	37.91	**3.11**	**38.80**
10	9.60	28.51	5.94	32.79	6.69	31.69	5.48	33.56	**5.13**	**34.22**
15	14.31	25.04	8.01	30.16	8.91	29.18	7.43	30.90	**6.98**	**31.43**
20	18.88	22.63	9.90	28.31	11.06	27.31	9.39	28.81	**8.71**	**29.47**
25	23.40	20.77	11.65	26.90	13.14	25.83	11.45	27.08	**10.36**	**27.93**
30	27.77	19.28	13.42	25.67	15.33	24.50	13.59	25.59	**11.97**	**26.66**
Avg.	16.47	25.11	8.75	30.18	9.90	29.03	8.45	30.64	**7.71**	**31.42**

For each s.d., the averages of both the RMSE and the PSNR over all images are displayed.

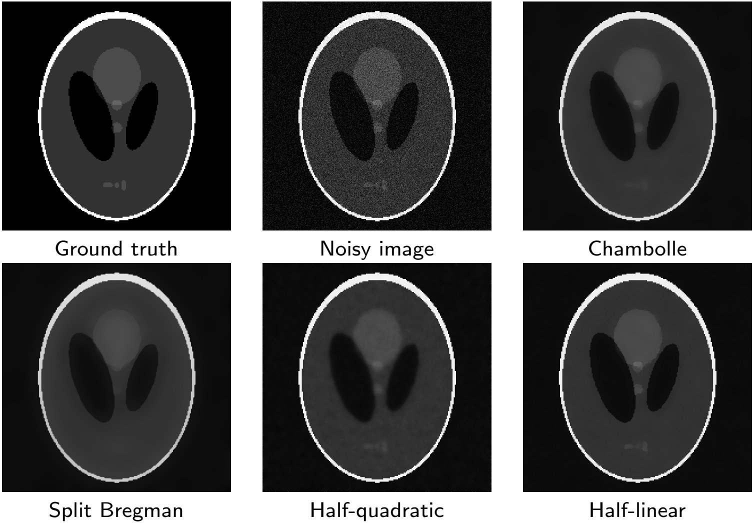

Figure : Denoising of piecewise constant image corrupted with Gaussian noise of s.d. $\sigma = 30$

Noisy image

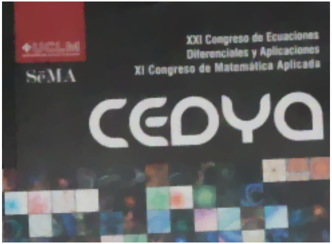

Chambolle

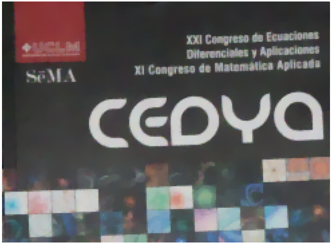

Split Bregman

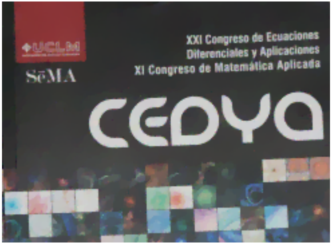

Half-linear

Figure : Denoising of a color non-constant image corrupted with Gaussian noise of s.d. $\sigma = 15$

Contents

A nonlocal variational model for pansharpening image fusion

The pansharpening problem

- Satellite data $\begin{cases} \text{high-resolution } \textbf{panchromatic image} \text{ (PAN)}, \\ \text{low-resolution } \textbf{multispectral image} \text{ (MS)}. \end{cases}$
- Sensor design → inverse relation between **spectral** and **spatial resolutions**.
- **Applications** → remote sensing (detection and classification), astronomy, military tasks, soil measure content, improving geometric correction, enhancing features...

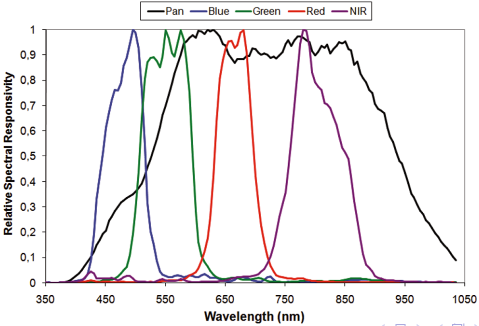

Panchromatic image

+

Low-resolution image

=

Pansharpened image

Truth image

IHS pansharpened image

A nonlocal variational model for pansharpening image fusion

The proposed nonlocal functional

Notations:

- $\Omega \subset \mathbb{R}^N$ open and bounded domain.
- $S \subseteq \Omega$ sampling grid (low-resolution pixels).
- PAN image: $P : \Omega \to \mathbb{R}$.
- MS image: $\vec{u}^S = (u_1^S, \ldots, u_M^S)$, $u_m^S : S \to \mathbb{R}$, M spectral bands.
- Pansharpened image: $\vec{u} = (u_1, \ldots, u_M)$, $u_m : \Omega \to \mathbb{R}$.

Goal $\to$ Obtain $\vec{u}$ from P and $\vec{u}^S$ as the minimizer of a functional.

Panchromatic matching term

- **Assumption**: PAN is a linear combination of multispectral channels.
- **Constraint**:

$$P(x) = \underbrace{\sum_{m=1}^{M} \alpha_m u_m(x),}_{\text{intensity of } \vec{u}} \quad \forall x \in \Omega,$$

  where $\alpha_m \geq 0$ and $\sum_m \alpha_m = 1$.

- **Energy term**:

$$\boxed{\int_\Omega \left(\sum_{m=1}^{M} \alpha_m u_m(x) - P(x) \right)^2 dx}$$

Spectral correlation preserving term

- **Assumption**: Low-resolution pixels formed from high-resolution ones by low-pass filtering followed by subsampling.
- **Constraint**: $u_m^S(x) = k_m * u_m(x), \quad \forall x \in S, \quad \forall 1 \leq m \leq M.$
- **Energy term**:

$$\sum_{m=1}^{M} \int_{\Omega} \Pi_S \cdot \left(k_m * u_m(x) - u_m^{\Omega}(x) \right)^2 dx$$

$k_m \rightarrow$ kernel of a convolution operator mapping $L^2(\Omega)$ into $\mathcal{C}(\bar{\Omega})$.

$u_m^{\Omega} \rightarrow$ arbitrary continuous extension of u_m^S from S to Ω.

$\Pi_S = \sum_{(i,j) \in S} \delta_{(i,j)} \rightarrow$ **Dirac's comb** defined by sampling grid S.

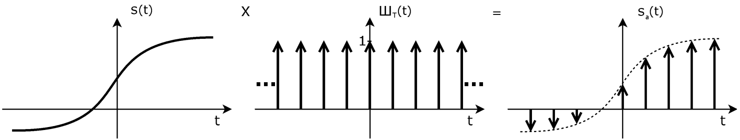

Nonlocal geometry enforcing term

Key → Introduce the geometry of PAN into MS using neighborhood filters

- Distances computed on PAN.
- **Weights**:

$$\omega(x,y) = \frac{1}{C(x)} e^{-\frac{d_\rho(P(x),P(y))}{h^2}}, \quad \underbrace{C(x) = \int_\Omega e^{-\frac{d_\rho(P(x),P(y))}{h^2}} dy,}_{\text{normalizing factor}}$$

$$d_\rho\left(P(x), P(y)\right) = \int_\Omega G_\rho(t) \left|P(x+t) - P(y+t)\right|^2 dt,$$

s.t. $0 \le \omega(x,y) \le 1$ and $\int_\Omega \omega(x,y) dy = 1 \ \forall x \in \Omega$.

- Weights are **non-symmetric** due to $C(x)$.
- **Energy term**:

$$\sum_{m=1}^{M} \int_\Omega \int_\Omega \left(u_m(x) - u_m(y)\right)^2 \omega(x,y) dx dy.$$

We propose to study the following **nonlocal energy functional**

$$\begin{aligned} J(\vec{u}) &= \frac{1}{2}\sum_{m=1}^{M}\int_\Omega\int_\Omega \left(u_m(x)-u_m(y)\right)^2\omega(x,y)dxdy \\ &+ \frac{\lambda}{2}\int_\Omega\left(\sum_{m=1}^{M}\alpha_m u_m(x)-P(x)\right)^2 dx \\ &+ \frac{\mu}{2}\sum_{m=1}^{M}\int_\Omega \Pi_S\cdot\left(k_m * u_m(x)-u_m^\Omega(x)\right)^2 dx, \end{aligned}$$

where $\lambda, \mu > 0$ are trade-off parameters experimentally fixed.

A nonlocal variational model for pansharpening image fusion

Theoretical analysis of the functional

- Assume $P \in L^2(\Omega)$ and $u_m^\Omega \in L^2(\Omega)$ $\forall 1 \leq m \leq M$.
- Is it $u_m \in L^2(\Omega)$ enough? $\rightarrow$ **nonlocal gradient** depending on ω:

$$\int_\Omega \int_\Omega \big(u_m(x) - u_m(y)\big)^2 \omega(x,y)dxdy < +\infty, \quad \forall 1 \leq m \leq M.$$

- **Nonlocal domain** $\rightarrow$ $\tilde{\Omega} = \Omega \cup \Gamma, \Gamma \subset \mathbb{R}^N \setminus \Omega$ surrounding Ω s.t. $|\Gamma| \neq 0$.
- **Solution space** $\rightarrow$ Weighted L^2 space:

$$L^2_\omega(\tilde{\Omega}\times\tilde{\Omega}) = \left\{ f : \tilde{\Omega}\times\tilde{\Omega} \rightarrow \mathbb{R} : f \text{ measurable. } \int_{\tilde{\Omega}} \int_{\tilde{\Omega}} |f(x,y)|^2 \omega(x,y)dxdy < +\infty \right\}$$

Theorem (Existence and uniqueness of minimizer)

If $\vec{g} = (g_1, \ldots, g_M)$, with $g_m \in L^2(\Gamma)$, then $\exists! \, \vec{u}^* \in \mathcal{A}$ s.t. $J(\vec{u}^*) = \inf_{\vec{u}\in\mathcal{A}} J(\vec{u})$.

A nonlocal variational model for pansharpening image fusion
Discrete details

- The algorithm consists in applying the **gradient descent method** to solve the **Euler-Lagrange equation**:

$$\int_{\widetilde{\Omega}} \big(u_k(x) - u_k(y)\big)\big(\omega(x,y) + \omega(y,x)\big)dy + \lambda\alpha_k \left(\sum_{m=1}^{M} \alpha_m u_m(x) - P(x)\right)$$
$$+ \mu k_k^{\intercal} * \left[\Pi_S \cdot \left(k_k * u_k(x) - u_k^{\Omega}(x)\right)\right] = 0, \quad \forall x \in \Omega.$$

- **Discrete weights** restricted to pixels at certain distance (support zone):

$$\omega(p,q) = \begin{cases} \dfrac{1}{C(p)} e^{-\frac{1}{h^2}\sum_{t\in\mathcal{N}_0}\|P(p+t)-P(q+t)\|^2}, & \text{if } \|p-q\| \leq L, \\ 0, & \text{otherwise,} \end{cases}$$

where $\mathcal{N}_0$ is an $l \times l$ window centered at $(0,0)$ (comparison window).

- **Normalizing factor**:

$$C(p) = \sum_{\{q:\|p-q\|\leq L\}} e^{-\frac{1}{h^2}\sum_{t\in\mathcal{N}_0}\|P(p+t)-P(q+t)\|^2}.$$

A nonlocal variational model for pansharpening image fusion

Experimental results

Comparison on natural images

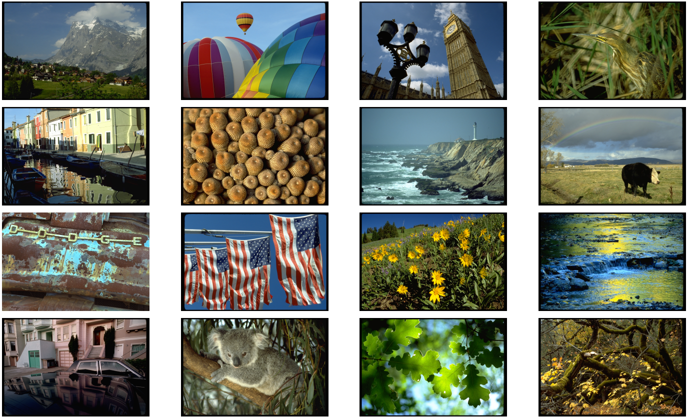

$s=2$					$s=4$				
IHS	Brovey	Waves	P+XS	NL	IHS	Brovey	Waves	P+XS	NL
1.23	1.10	2.23	1.36	**0.87**	2.00	1.84	2.62	1.95	**1.41**
1.40	1.39	3.46	1.72	**0.91**	2.74	2.71	4.01	2.68	**1.44**
1.27	1.25	2.46	1.51	**0.92**	2.08	2.04	2.90	2.10	**1.45**
1.09	1.05	2.35	1.35	**0.92**	1.95	1.85	2.77	1.96	**1.32**
2.11	2.09	3.80	2.16	**1.37**	3.43	3.40	4.45	3.41	**2.40**
1.83	1.79	3.29	2.30	**1.25**	2.89	2.80	3.72	3.01	**2.23**
1.10	1.09	1.88	1.27	**0.88**	1.66	1.63	2.26	1.70	**1.30**
1.03	1.00	1.99	1.29	**0.82**	1.66	1.62	2.37	1.74	**1.27**
2.05	2.06	4.19	2.67	**1.55**	3.70	3.70	4.91	3.95	**2.50**
2.27	2.22	5.77	2.60	**1.50**	4.51	4.43	6.62	4.41	**2.55**
3.87	3.38	7.33	3.72	**1.65**	6.59	5.93	8.37	5.95	**3.81**
3.50	3.44	6.86	4.58	**2.03**	6.38	6.31	7.91	6.93	**4.65**
0.93	0.93	1.69	1.03	**0.78**	1.47	1.46	2.07	1.49	**1.15**
1.16	1.14	2.33	1.49	**0.97**	2.07	2.05	2.79	2.17	**1.47**
2.05	1.87	4.12	1.99	**1.44**	3.25	3.06	4.65	3.04	**2.10**
2.77	2.57	5.33	3.41	**1.48**	4.80	4.54	6.10	4.91	**3.03**
1.85	1.77	3.69	2.15	**1.21**	3.20	3.09	4.28	3.21	**2.13**

Truth image

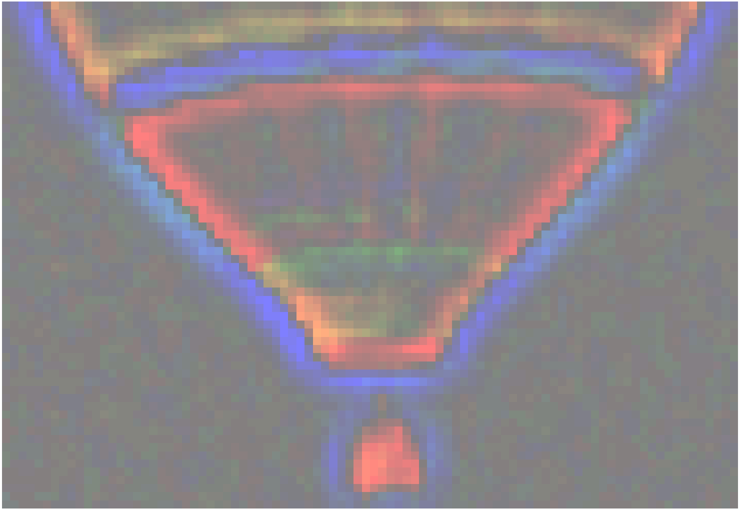

IHS pansharpened image

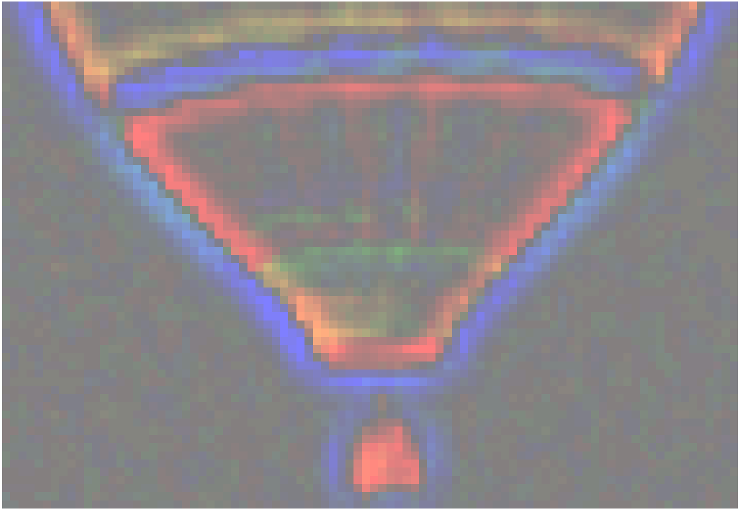

Brovey pansharpened image

Wavelets-based pansharpened image

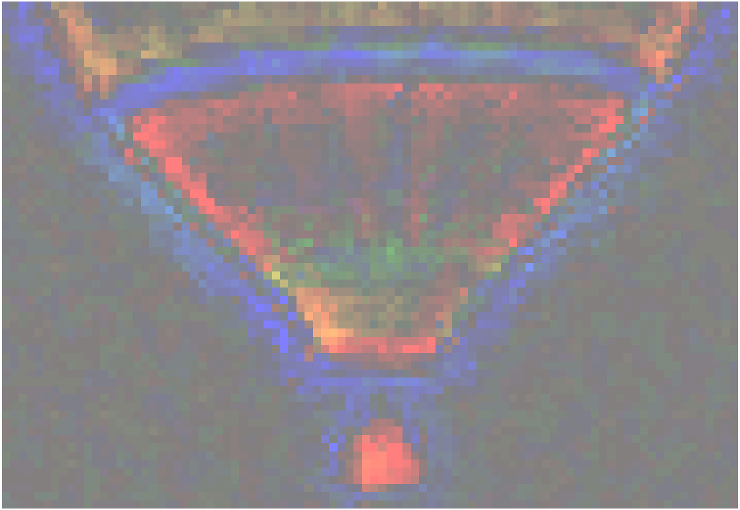

P+XS pansharpened image

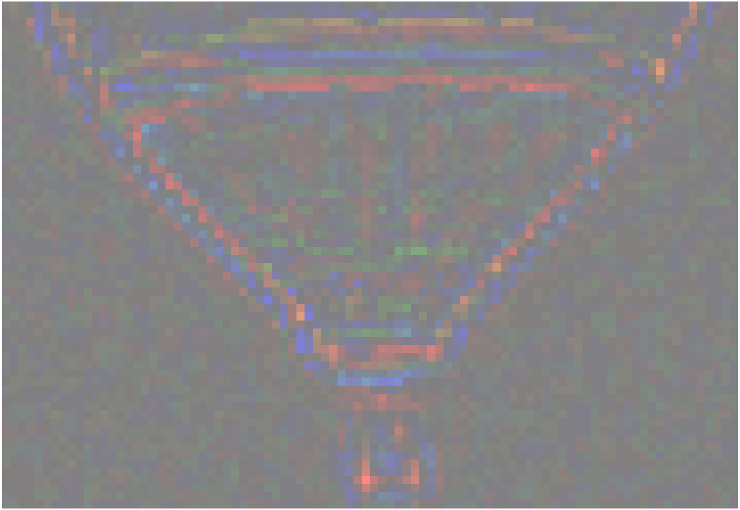

Nonlocal pansharpened image

Comparison on aerial images

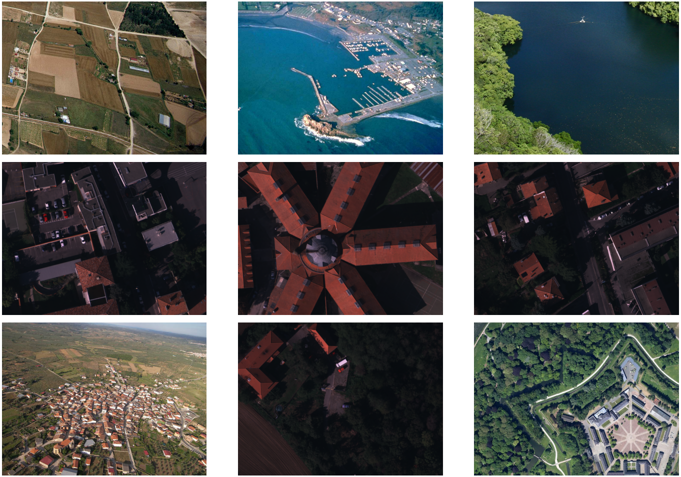

$s=2$					$s=4$				
IHS	Brovey	Waves	P+XS	NL	IHS	Brovey	Waves	P+XS	NL
1.16	1.14	1.80	1.54	**1.05**	1.93	1.91	2.26	2.15	**1.60**
1.42	1.40	2.58	1.97	**1.37**	2.23	2.21	2.96	2.64	**1.83**
1.03	0.99	1.90	1.43	**0.87**	1.72	1.68	2.17	1.94	**1.34**
2.08	2.07	2.71	1.92	**1.68**	2.62	2.62	2.89	2.54	**2.26**
2.43	2.43	3.21	2.24	**2.10**	3.02	3.02	3.44	2.86	**2.52**
1.42	1.41	1.96	1.26	**1.18**	1.83	1.82	2.11	1.70	**1.49**
1.75	1.74	2.92	2.46	**1.45**	3.04	3.03	3.68	3.47	**2.29**
0.99	0.98	1.46	0.88	**0.82**	1.33	1.32	1.59	1.22	**1.04**
1.27	1.25	2.36	1.95	**1.14**	2.21	2.20	2.86	2.60	**1.63**
1.51	1.49	2.32	1.74	**1.30**	2.21	2.20	2.66	2.35	**1.78**

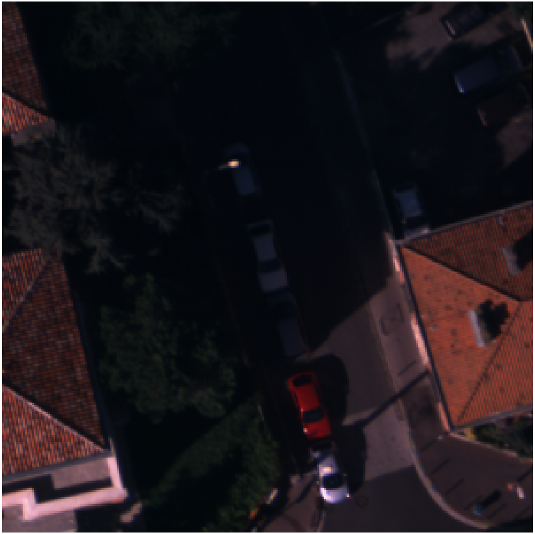

Truth image

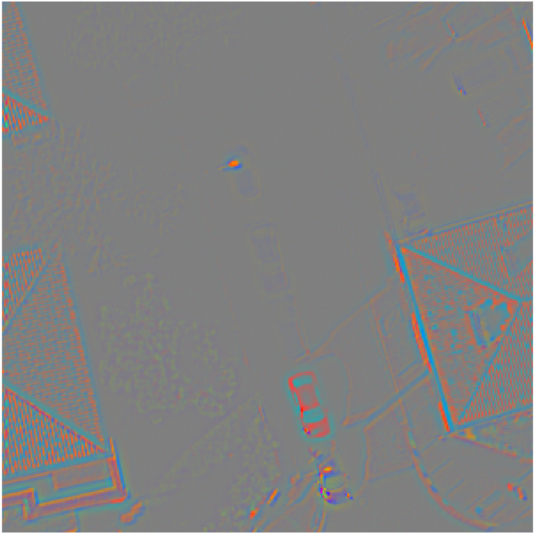

IHS pansharpened image

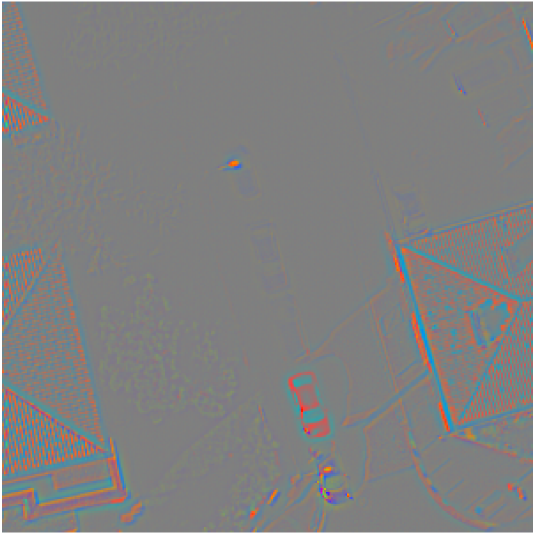

Brovey pansharpened image

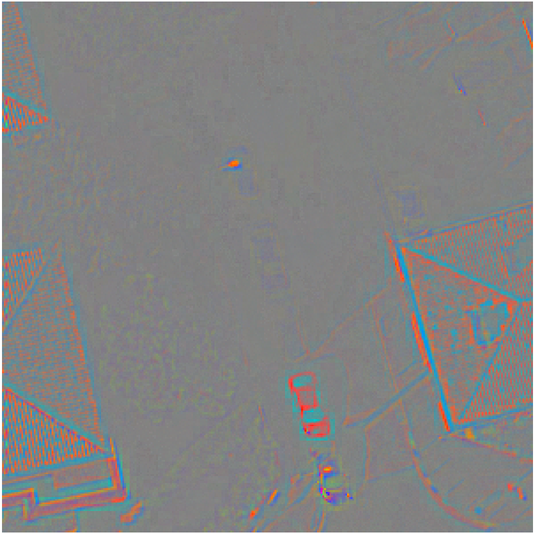

Wavelets-based pansharpened image

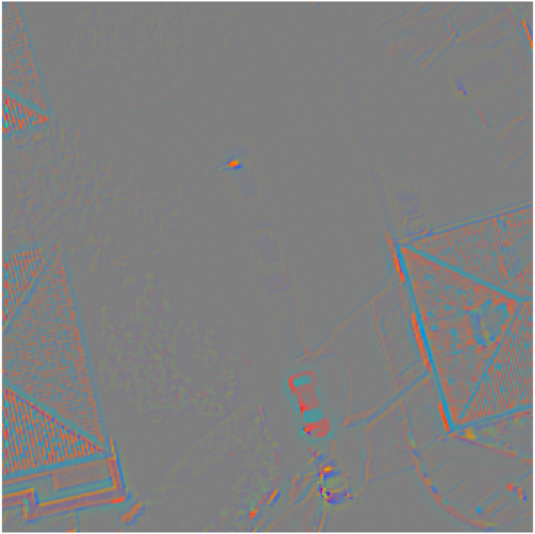

P+XS pansharpened image

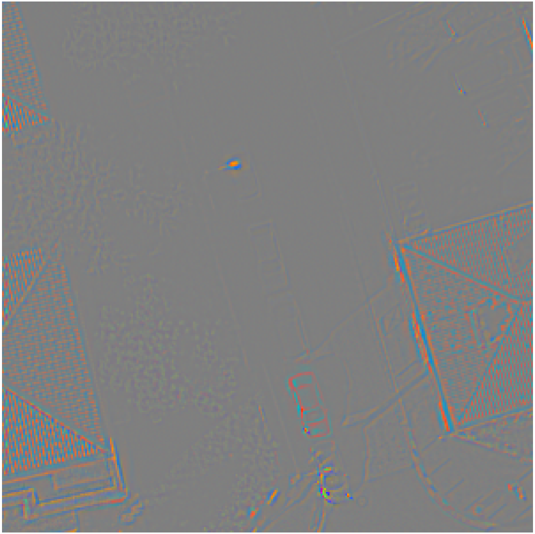

Nonlocal pansharpened image

Comparison on satellite images

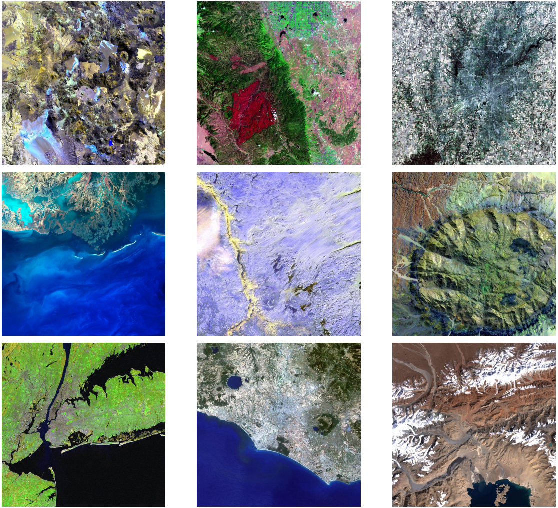

$s = 2$					$s = 4$				
IHS	Brovey	Waves	PXS	Ours	IHS	Brovey	Waves	PXS	Ours
2.31	2.38	3.99	3.24	**1.64**	4.01	4.04	4.87	4.53	**2.90**
3.78	3.81	6.35	5.11	**2.53**	6.45	6.45	7.49	7.07	**4.96**
1.41	1.55	2.08	1.97	**1.05**	2.34	2.42	2.70	2.69	**1.79**
2.93	2.99	4.94	3.71	**1.99**	4.96	4.99	5.80	5.27	**3.80**
1.50	1.59	2.45	2.09	**1.35**	2.49	2.53	3.03	2.86	**1.96**
1.62	1.74	2.65	2.31	**1.47**	2.78	2.85	3.37	3.21	**2.18**
2.90	2.94	5.08	4.04	**1.91**	5.12	5.11	6.09	5.65	**3.69**
0.89	1.11	1.30	1.30	**0.75**	1.40	1.55	1.66	1.68	**1.15**
1.14	1.31	1.73	1.57	**1.05**	1.84	1.94	2.20	2.10	**1.48**
2.05	2.16	3.40	2.82	**1.53**	3.49	3.54	4.13	3.90	**2.66**

Truth image

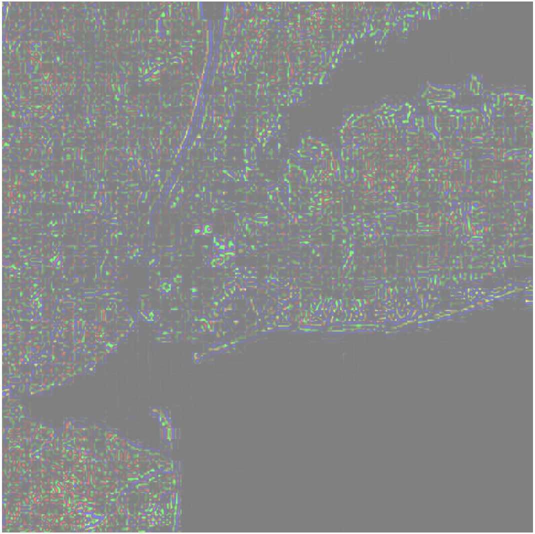

IHS pansharpened image

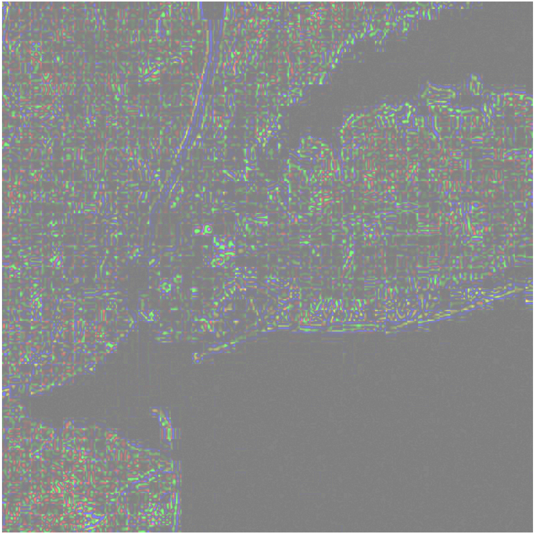

Brovey pansharpened image

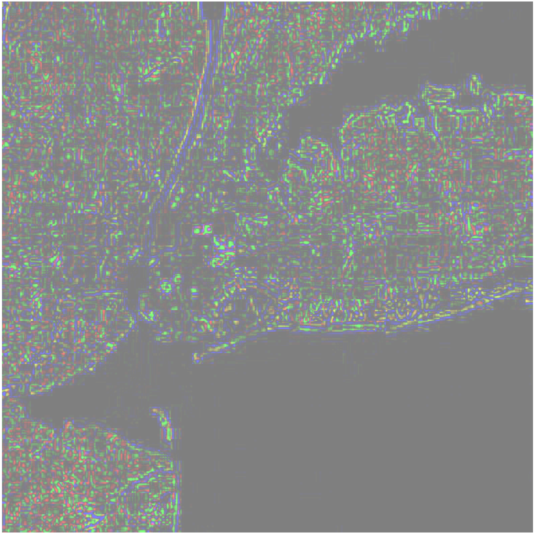

Wavelets-based pansharpened image

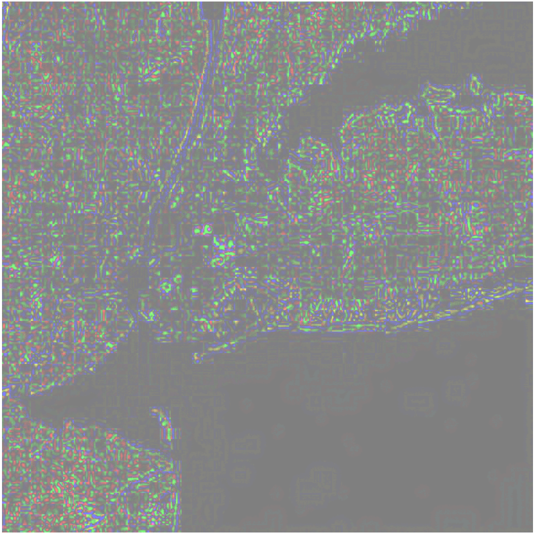

P+XS pansharpened image

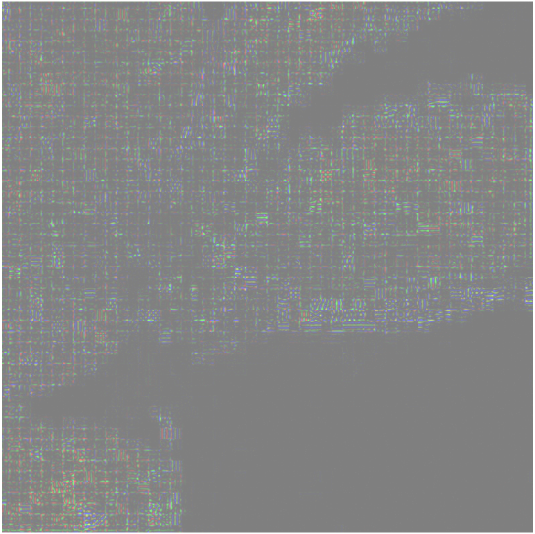

Nonlocal pansharpened image

Truth color image

Initial color image by replication

Nonlocal pansharpened color image

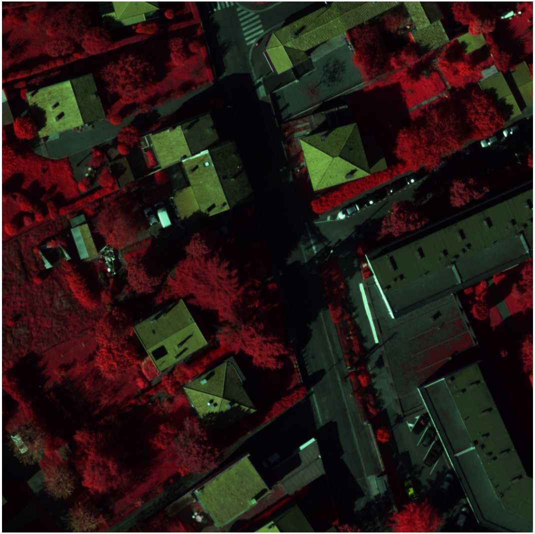

Truth false color image

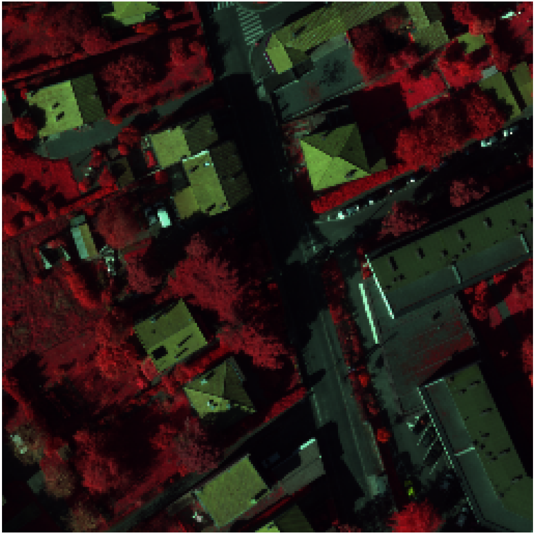

Initial false color image by replication

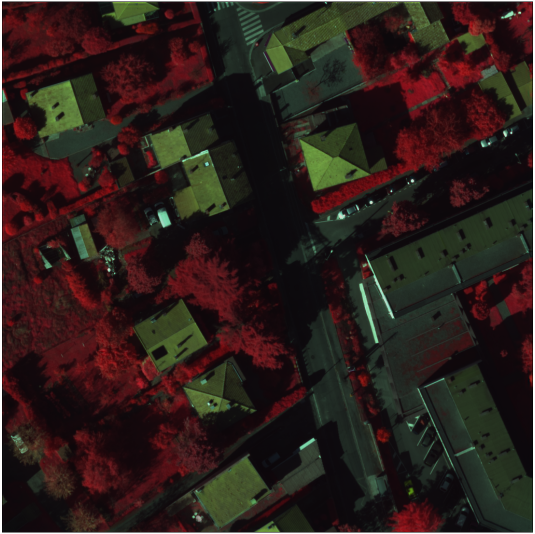

Nonlocal pansharpened false color image

Contents

Self-similarity and spectral correlation adaptive image demosaicking

The demosaicking problem

- Most common cameras use CCD sensor devices measuring a single color per pixel.
- **Demosaicking** $\rightarrow$ interpolate the two missing values from the neighboring ones.
- **CFA** $\rightarrow$ Bayer color filter array

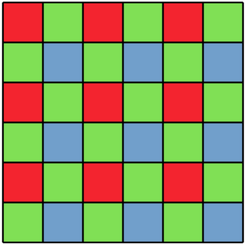

- Subsampling of factor 4 for red and blue, and of factor 2 for green.
- Equal horizontal and vertical sampling frequency for each color.

Mosaicked image

Demosaicked image

Self-similarity and spectral correlation adaptive image demosaicking

State-of-the-art demosaicking techniques

- Interpolation of **green channel** $\rightarrow$ easier reconstruction of geometry and texture:
  - Local estimation of the most suitable direction of interpolation
  - Take a decision *a priori* or *a posteriori*.
  - Combine different directional estimations.
- Interpolation of **red and blue channels** $\rightarrow$ estimate the ratios $G - R$ and $G - B$ due to channel inter-correlation.
- **Iterative algorithms** $\rightarrow$ starting with an initial condition, iteratively force the three color channels to have the same high frequencies or to have low cost-energy.
- **Databases:**
  - Kodak $\rightarrow$ fewer color saturated regions and large inter-channel correlation.
  - IMAX $\rightarrow$ many more saturated colors and edges separating colored regions and lower inter-channel correlation.

Self-similarity and spectral correlation adaptive image demosaicking

Local directional interpolation with a posteriori decision

i) Interpolate the green channel along four directions:

$$\widehat{G}^n_{i,j} = C_{i,j} + d^n_{i,j} = G_{i,j-1} + \frac{\beta}{2}\left(C_{i,j} - C_{i,j-2}\right),$$

where $0 < \beta \leq 1$ balances the assumption on chromatic regularity.

ii) Estimate red and blue channels by bilinear interpolation of the differences:

$$CG^n_{i,j} = C_{i,j} - \beta G^n_{i,j} \;\rightarrow\; \widehat{C}^n_{i,j} = \widehat{CG}^n_{i,j} + \beta G^n_{i,j}.$$

iii) Weight the four fully color images in terms of the chromatic variances in the YUV space:

$$\begin{aligned} R &= \omega^n R^n + \omega^s R^s + \omega^e R^e + \omega^w R^w \\ G &= \omega^n G^n + \omega^s G^s + \omega^e G^e + \omega^w G^w \\ B &= \omega^n B^n + \omega^s B^s + \omega^e B^e + \omega^w B^w \end{aligned}$$

The channel correlation parameter β is computed empirically

Self-similarity and spectral correlation adaptive image demosaicking

Nonlocal filtering of channel differences

- Local regularity of the image → color artifacts and erroneous interpolations.
- Exploit the image self-similarity to correct them.
- The weight distribution is computed on the initial interpolated image:

$$\omega(x,y) = \frac{1}{\Psi(x)} e^{-\frac{d(\mathbf{u_0}(x),\mathbf{u_0}(y))}{h^2}}, \quad \Psi(x) = \sum_{y\in\Omega} e^{-\frac{d(\mathbf{u_0}(x),\mathbf{u_0}(y))}{h^2}}$$

- Apply nonlocal regularity to channel differences at unknown pixels.
  i) Green filtering:

$$G(x) = \sum_{y\in\Omega} \omega(x,y)\left(G_0(y) - \beta C_0(y)\right) + \beta C_0(x), \quad x \notin \Omega_G.$$

  ii) Red and Blue filtering taking advanced of already filled green:

$$C(x) = \sum_{y\in\Omega} \omega(x,y)\left(C_0(y) - \beta G(y)\right) + \beta G(x), \quad x \notin \Omega_C.$$

Self-similarity and spectral correlation adaptive image demosaicking

Experimental results

Kodak database

IMAX database

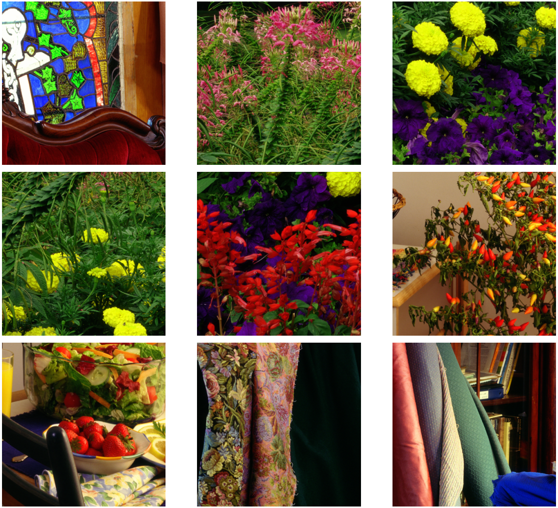

Digital photographs

	HA	DLMMSE	SSD	LDNAT	CS	Ours
1	5.14	2.63	4.17	4.36	2.36	**2.30**
2	2.41	1.86	2.00	2.02	1.79	**1.71**
3	4.50	2.33	3.56	4.03	2.51	**2.30**
4	2.34	1.99	2.14	2.15	**1.97**	2.04
5	4.31	2.59	3.56	4.03	2.45	**2.45**
6	2.08	1.77	2.04	1.99	**1.84**	1.85
7	2.44	1.79	2.19	2.37	1.87	**1.73**
8	2.96	2.00	2.62	2.80	2.15	**1.99**
9	3.41	2.19	2.96	3.26	2.40	**2.12**
Avg	3.29	2.13	2.80	3.00	2.15	**2.05**

Table : RMSE of images in Kodak database

	HA	DLMMSE	SSD	LDNAT	CS	Ours
1	9.22	10.34	9.36	**7.69**	7.72	7.89
2	9.19	10.52	9.61	8.02	8.52	**8.01**
3	5.88	6.95	5.91	**4.58**	4.80	4.77
4	6.34	7.33	6.55	**5.17**	6.05	5.32
5	5.38	6.88	5.31	4.37	**4.29**	4.42
6	5.90	7.16	5.96	**4.76**	5.38	5.07
7	4.37	5.22	4.32	**3.62**	4.01	3.86
8	5.21	5.90	5.26	**4.43**	5.25	4.54
9	4.77	4.91	4.65	**4.26**	4.66	4.55
Avg	6.25	7.25	6.33	**5.21**	5.63	5.38

Table : RMSE of images in IMAX database

	HA	DLMMSE	SSD	LDNAT	CS	Ours
Avg	4.77	4.69	4.57	4.11	3.89	**3.72**

Table : RMSE average of images in Kodak and IMAX databases

	HA	DLMMSE	SSD	LDNAT	CS	Ours
1	1.77	**1.50**	1.79	1.75	1.56	1.62
2	7.35	4.67	5.91	6.56	4.65	**4.22**
3	3.21	2.09	2.61	2.81	2.15	**2.01**
4	3.90	3.45	3.58	3.64	**3.36**	3.42
5	4.64	2.46	3.48	3.96	2.49	**2.23**
6	7.43	4.29	5.35	6.66	3.60	**3.42**
7	3.91	2.31	3.15	3.75	2.07	**2.02**
8	6.16	3.35	4.34	5.34	3.80	**2.48**
9	4.65	2.95	3.60	4.38	2.81	**2.61**
Avg	4.78	3.01	3.76	4.32	2.94	**2.67**

Table : RMSE of images in digital photographs collection

Truth image

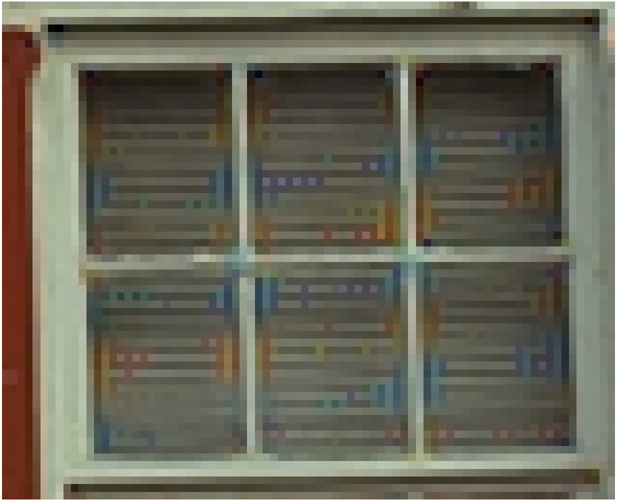

HA demosaicked image

DLMMSE demosaicked image

SSD demosaicked image

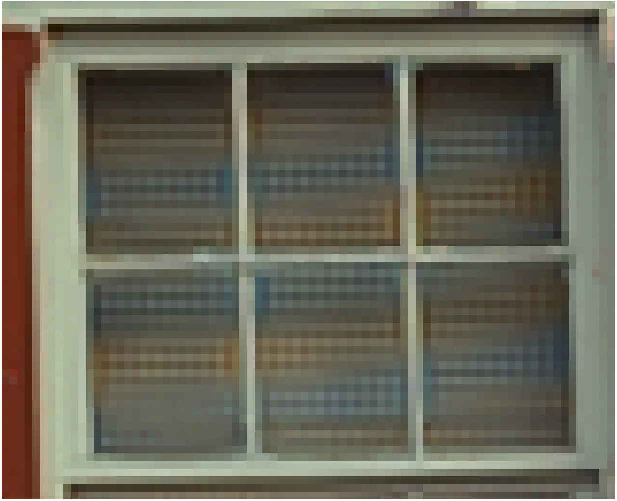

LDNAT demosiacked image

CS demosaicked image


Our demosaicked image

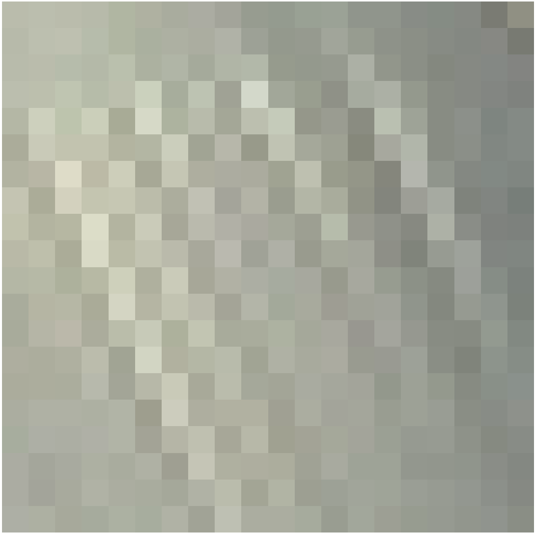

Truth image

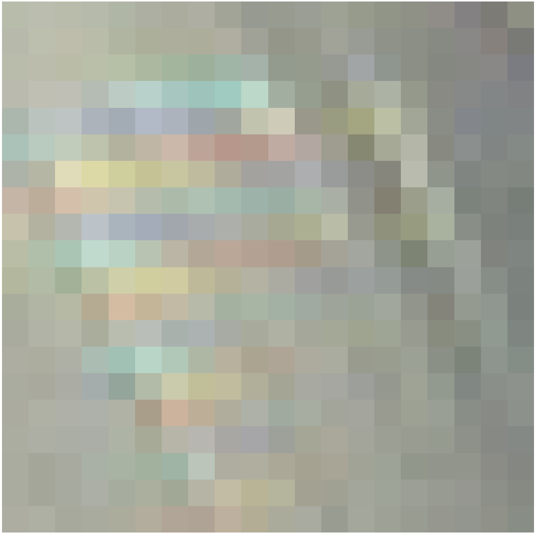

HA demosaicked image

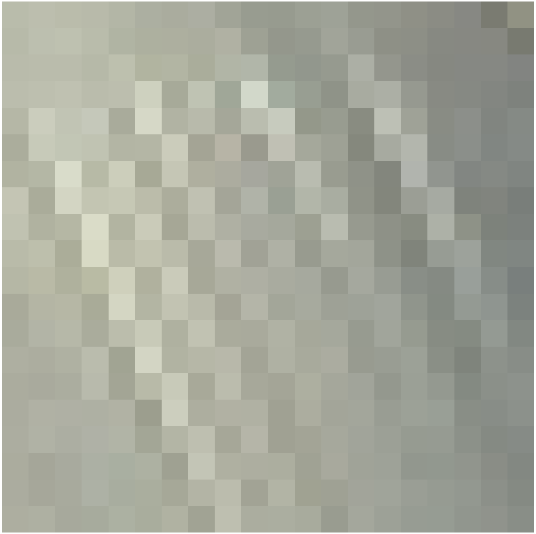

DLMMSE demosaicked image

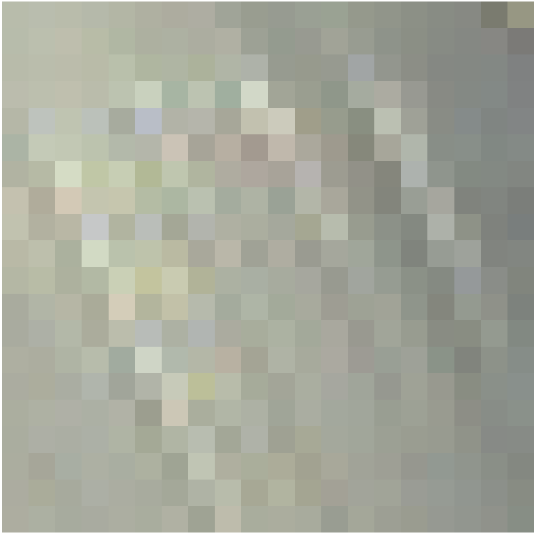

SSD demosaicked image

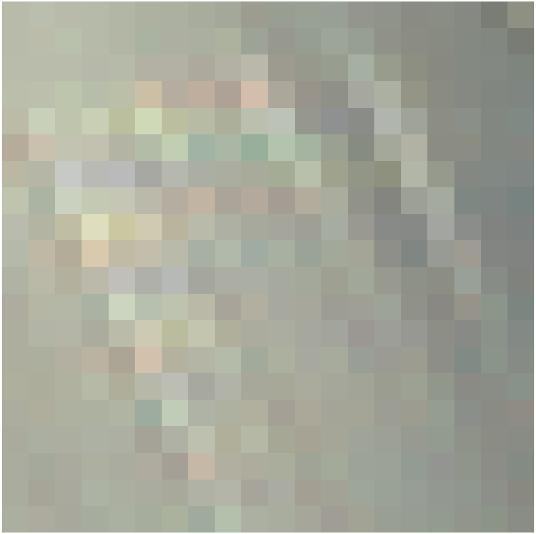

LDNAT demosiacked image

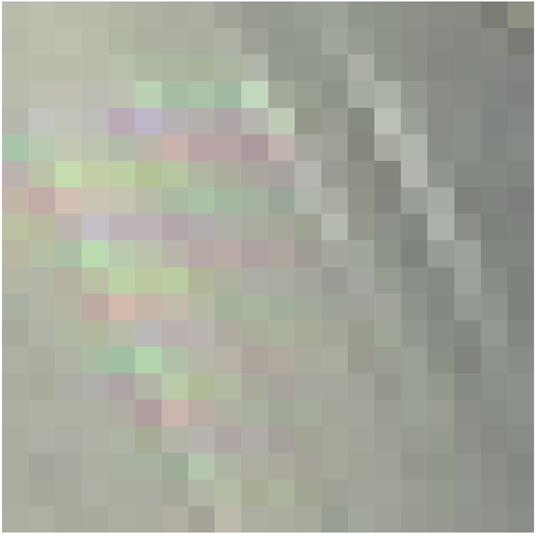

CS demosaicked image

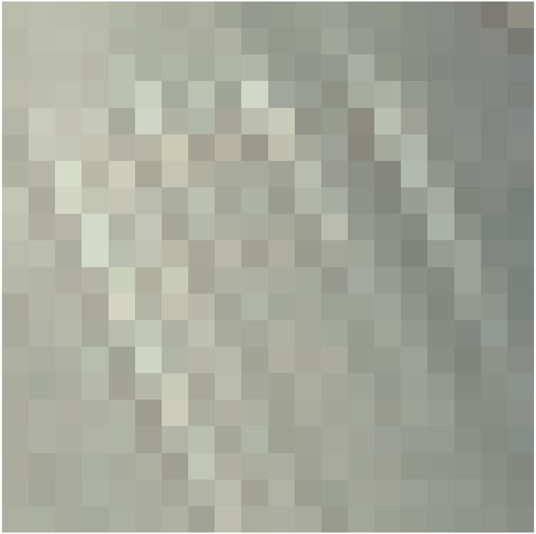

Our demosaicked image

Truth image

HA demosaicked image

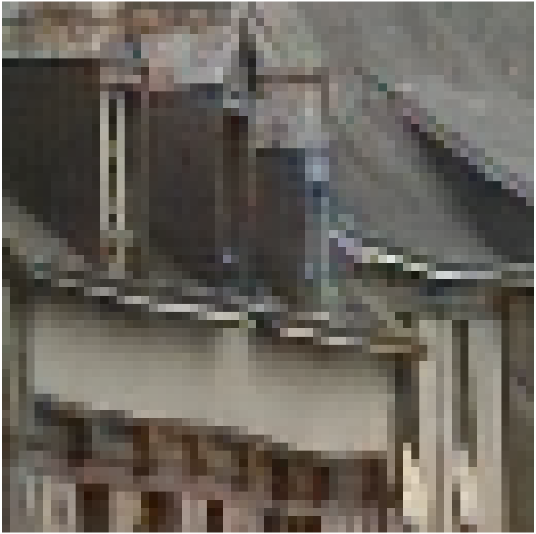

DLMMSE demosaicked image

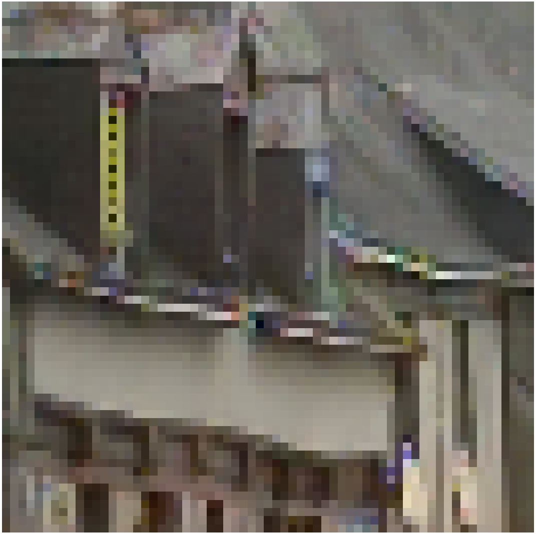

SSD demosaicked image

LDNAT demosiacked image

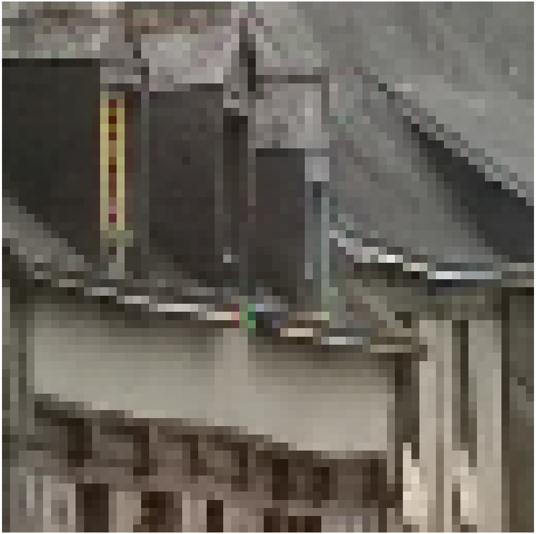

CS demosaicked image

Our demosaicked image

Contents

Future work and references

Future work

- Adapt nonlocal pansharpening algorithm to Pléiades images.
- Improve demosaicking algorithm.
- Texture synthesis and texture segmentation.
- Video and multiview reconstruction.

References

- J. Duran, B. Coll, C. Sbert. *Chambolle's projection algorithm for total variation denoising*. Image Process. On Line, 3:311-331, 2013.
- J. Duran, A. Buades, B. Coll, C. Sbert. *Implementation of nonlocal pansharpening image fusion*. Image Process. On Line, 4:1-15, 2014.
- J. Duran, A. Buades, B. Coll, C. Sbert. *A nonlocal variational model for pansharpening image fusion*. SIAM J. Imaging Sci., 7(2):761-796, 2014.
- B. Coll, J. Duran, C. Sbert. *An algorithm for nonconvex functional minimization and applications to image restoration*. In Proc. of IEEE Int. Conf. Image Process. 2014 (ICIP), Paris, 2014.
- B. Coll, J. Duran, C.Sbert. *Half-linear regularization for nonconvex image restoration models*. Submitted to AIMS Inverse Problems and Imaging, 2014.
- J. Duran, A. Buades. *Self-similarity and spectral correlation adaptive algorithm for color demosaicking*. Submitted to IEEE Trans. Image Process., 2014.